



HAL
open science

Impact of edge morphology and chemistry on nanoribbons' gapwidth

Elisa Serrano Richaud, Sylvain Latil, Lorenzo Sponza

► **To cite this version:**

Elisa Serrano Richaud, Sylvain Latil, Lorenzo Sponza. Impact of edge morphology and chemistry on nanoribbons' gapwidth. 2023. hal-04290277

HAL Id: hal-04290277

<https://hal.science/hal-04290277>

Preprint submitted on 16 Nov 2023

HAL is a multi-disciplinary open access archive for the deposit and dissemination of scientific research documents, whether they are published or not. The documents may come from teaching and research institutions in France or abroad, or from public or private research centers.

L'archive ouverte pluridisciplinaire **HAL**, est destinée au dépôt et à la diffusion de documents scientifiques de niveau recherche, publiés ou non, émanant des établissements d'enseignement et de recherche français ou étrangers, des laboratoires publics ou privés.

Impact of edge morphology and chemistry on nanoribbons' gapwidth

Elisa Serrano Richaud,¹ Sylvain Latil,² and Lorenzo Sponza^{1,3}

¹ *Université Paris-Saclay, ONERA, CNRS, Laboratoire d'étude des microstructures, 92322, Châtillon, France*

² *Université Paris-Saclay, CEA, CNRS, SPEC, 91191 Gif-sur-Yvette, France*

³ *European Theoretical Spectroscopy Facility (ETSF), B-4000 Sart Tilman, Liège, Belgium*

(Dated: today)

In this work, we scrutinise theoretically how the gap of C and BN armchair nanoribbons changes upon variations of the bond length between edge atoms and their distance from passivating species. Our DFT calculations indicate that the gap of C-based nanoribbons is more sensitive to the relaxation of the bonding length between edge atoms (morphology) whereas in BN-nanoribbons it is more sensitive to the distance between edge atoms and passivating hydrogens (chemical environment). To understand the origin of these two different behaviours, we solved a tight-binding ladder model numerically and at the first-order perturbation theory, demonstrating that the different dependence is due to the interference of the wavefunctions of the top valence and the bottom conduction states.

I. INTRODUCTION

In recent decades, graphene and hexagonal boron nitride (BN) have attracted a great deal of interest because of their remarkable transport and optical properties¹⁻⁵. A much explored way to modulate them is by adding extra confinement (as in 2D quantum dots, nanoribbons or nanotubes). The presence of confining edges endows them with novel size-dependent features dominated by the characteristics of the edge itself. This is why graphene and BN nanoribbons are often classified according to their edge shape, which can be zig-zag, armchair, fall in an intermediate chiral angle, or present structures that require a more general nomenclature⁶. In zig-zag nanoribbons, well localised edge-state are formed which confer antiferromagnetic properties to C-based zig-zag nanoribbons⁶⁻¹². Instead, BN-based zig-zag nanoribbons have an indirect gap and display an intrinsic dipole moment^{9,13-19}. At variance, both graphene^{6,8-12,20-27} and BN^{9,14-18} armchair nanoribbons (AGNR and ABNNR), have no magnetic states and display a direct size-dependent gapwidth. To take full advantage of this richness of properties, several methods have been explored including the application of external electromagnetic fields^{9,10,14,18,27}, strain^{17,24,28} and edge engineering^{17,19,21-26,29}.

As a matter of fact, the edge characteristics are crucial for the performances of nanoribbon-based devices such as transistors, interconnects and logical devices^{23,29-33}, photovoltaic applications^{33,34}, or chemical sensing^{33,35}. Experimentally, edge engineering^{34,36,37}, chemical treatment³⁸ or selective passivation²⁹ have been demonstrated to have a significant impact on the device quality, precisely because of their action on the edges.

Alterations of the electronic structure due to edge modifications can be divided into morphology effects (variation of the bondlengths) and chemistry effects (variation of the passivating species and their distance from the edges)^{6,26}. The sensitivity of AGNR and ABNNR gap to the passivation has been investigated by many authors^{6,17,19,21-26,29} who showed that its effect depends on the type of atoms involved, and/or on the number and position of the passivated sites.

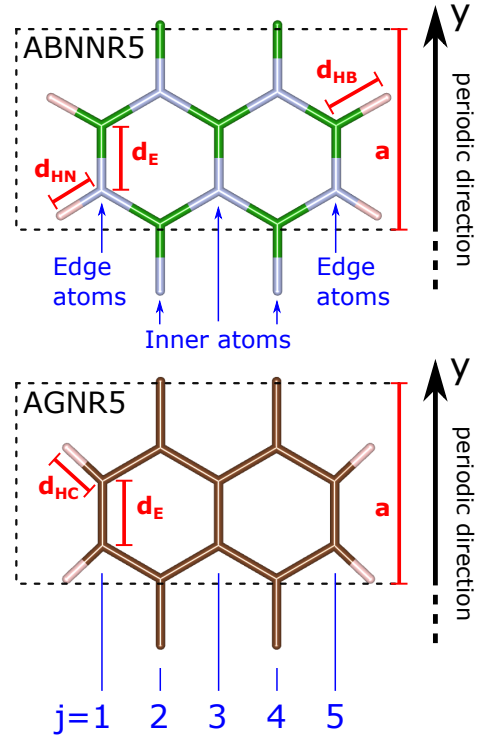


Figure 1. Scheme of relaxed AGNR5 and ABNNR5 structures. Unitary cells are reported as black dashed rectangles and some relevant structural parameters are labelled in red. In blue, the row index j and the edge or inner character of atoms are also reported.

Most of these first-principle studies^{17,19,21-25} discuss the role of passivation on fully relaxed structures, so morphology and chemistry effects are actually treated on the same footing. At best of our knowledge, only two studies^{6,26} have been conducted in frameworks that separate the two effects, but in both publications the focus is put on other aspects than the dependence of the gapwidth on morphology and chemistry modifications.

On the other hand, rare are the studies on genuine morphological effects^{6,12,26} and they are done only on AGNRs. Actually, in^{39,40}, a thorough study of edge reconstruction and edge stress in graphene and BN nanoribbons is actually carried out, but the investiga-

tion stops at a stability level and the relation to the gapwidth is not explored. However, both effects seem to be decisive in determining the gap of nanoribbons and we deemed that the subject deserved a more focused study.

In this article, we employ density functional theory (DFT) to study the evolution of the gap, the top valence (TV) and the bottom conduction (BC) states of AGNRs and ABNRs as a function of the nanoribbon size upon variations of the distance between edge atoms and between these and the passivating species. Our objective is to compare the effect of morphological and chemical variations on the gapwidth and understand which of them is dominant and in which situation. We demonstrate that the response of the gapwidth to changes of the distance between edge atoms (morphology) or between edge atoms and passivating atoms (chemical environment) is opposite in the two materials and we rationalise this different behaviour by means of a tight-binding model which we solved both numerically and perturbatively.

II. STRUCTURAL AND COMPUTATIONAL DETAILS

All nanoribbons studied in this article have armchair edges passivated with H atoms. They form an infinite periodic structure in the y direction and are confined along x . The extension of the periodic cell along y is the cell parameter a , while the width is expressed by the number N_a which indicates the number of dimers aligned along y inside the unitary cell (number of rows). To indicate a specific structure we will attach the index N_a after the label of the material, as in Figure 1, so for instance AGNR5 designates an armchair graphene nanoribbon of size $N_a = 5$.

Density functional theory calculations were carried out within the generalized gradient approximation using the PBE⁴¹ exchange correlation potential as implemented in the Quantum ESPRESSO⁴² simulation package. Long-range van der Waals corrections were included via the DFT-D2 method⁴³. To avoid interactions between consecutive cells, we included 15 Å and 20 Å of empty space in the z and x directions respectively. In electron density calculations and relaxation runs, the periodic axis was sampled with 20 k-points centered in Γ (corresponding to 11 irreducible k-points). This mesh was dense enough to converge total energies in the smallest nanoribbons. For density of states (DOS) calculations, a five times denser sampling was adopted for all systems and the resulting spectra have been broadened with a Gaussian distribution with a width of 0.02 eV.

We used norm-conserving pseudopotentials⁴⁴ and set the kinetic energy cutoff at 80 Ry in both materials. It is worth stressing that using a large vertical empty space and a high energy cutoff is essential even in the relaxation runs in order to prevent nearly free-electron states from hanging below the p_z states hence jeopardizing the gap description. In fact, as already well known for free-standing layers^{45–49} and

nanotubes^{50–52} in BN nanomaterials there is a competition at the bottom conduction between $2p_z$ and $3s$ states, whose right alignment requires a dedicated convergence study. If sometimes one can overlook this issue in BN layers, because the two competing states originate direct and indirect band gaps, this is not the case in ABNNRs where both states give rise to a direct gap at Γ .

In non-relaxed structures, all atoms occupy the sites of a regular honeycomb lattice with an inter-atomic distance of 1.42 Å. Structural relaxation runs have been performed with the Broyden–Fletcher–Goldfarb–Shanno (BFGS) algorithm for all systems with the stopping criterion of all forces being lower than 5×10^{-5} eV/Å. We allowed variations of the cell parameter a and all atomic positions. As clarified in the following, we also run some calculations letting only specific atoms to move. In Figure 1 we report the relaxed structures of AGNR and ABNNR at $N_a = 5$ for sake of example, and we introduce some notable structural parameters. In the AGNRs, the main modifications with respect to non-relaxed structures are a contraction of the distance between edge atoms d_E and between C and H d_{HC} . In ABNNR, we observe a similar contraction of the B–N distance on the edges d_E , and different contractions of the distances between H–B and H–N ($d_{HB} \neq d_{HN}$). We observed also that these modifications are basically independent on the size of the nanoribbon both qualitatively and quantitatively, so the structural parameters undergo minimal variations when comparing nanoribbons of different size.

III. GAP EDGE STATES

A. AGNRs

The electronic structure of AGNRs has been already studied in the past^{6,8–11,20–26,33,34}. Both non-relaxed and relaxed ribbons display a band gap at Γ of gapwidth Δ_{N_a} . Because of the 1D confinement, the gapwidth falls in one of the three families $N_a = 3m - 1$, $3m$ or $3m + 1$ (with $m \in \mathbb{N}^*$). Each family follows a different trend which asymptotically tends to zero for growing nanoribbon sizes and follows the general rule $\Delta_{3m-1} < \Delta_{3m} < \Delta_{3m+1}$. This is depicted in Figure 2 where we plot the gapwidth of AGNRs versus N_a for both non-relaxed and relaxed structures (red dashed and solid blue curves). The effect of relaxation is to open the gap by about 0.1 eV in families $N_a = 3m + 1$ and $3m - 1$, while in the $N_a = 3m$ the opening is observed only in small nanoribbons, while the gap closes in larger ones. Our results are in quantitative agreement with previous works both for relaxed^{11,12,21,25}, and unrelaxed simulations²⁶.

To characterise better the gap states, we analyzed in more detail the nature of the TV and the BC states at Γ in the relaxed structures. In panels a) and b) of Figure 3, we report the band structure and the density of states (DOS) of the AGNR8, chosen as a representative example. For sake of comparison, in panel b) we

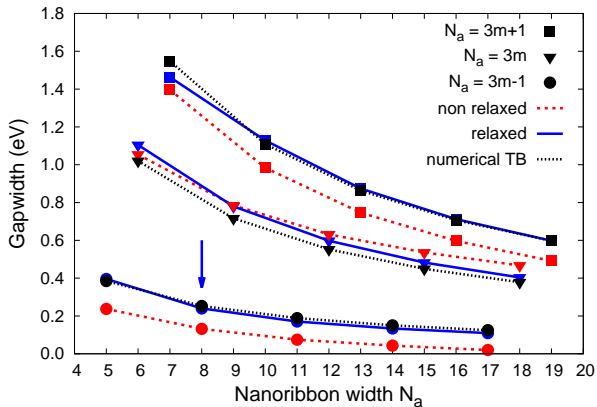


Figure 2. Energy gap of graphene nanoribbons as a function of the width N_a . Relaxed calculations (blue solid line), unrelaxed (red dashed line) and tight-binding numerical solution (black dotted) with parameters indicated in Table I. The three families are reported with different symbols. A blue arrow at $N_a = 8$ indicate the nanoribbon chosen for the analysis presented in Figure 3.

also report the orbital-projected DOS and the DOS of an infinite graphene sheet with the same inter-atomic distance. The DOS around the gap (from -1.5 eV to 1.5 eV) displays neat van Hove singularities arranged more or less symmetrically with respect to the middle of the gap. As the inset of panel b) shows clearly, the states composing the gap are entirely of p_z character. They form a π bonding with nodes on the xy plane, as expected. Instead, the first empty σ state is found at 3 eV above the BC. To go deeper in the analysis of the gap-edge states, we look at the site-projected DOS. We integrated the bare data inside an interval of 0.1 eV encompassing the TV and BC (shaded bands in the inset of Figure 3b). The outcome of this analysis is summarised in Figure 3c), where the site-projected DOS of gap-edge states is reported as a function of the row index (note that the curves are plotted on the same y axis). At variance from what observed in zigzag nanoribbons⁷, the gap states are not concentrated on the edge atoms, but rather delocalized throughout the full nanoribbon and present a modulation that nicely displays the characteristics of a static wave. This observation is confirmed by the wave-like modulation of the charge probability $|\psi(\mathbf{r})|^2$ associated with the TV and BC states, reported aside panel c). The wavefunction plot shows also that there is no spill-out on the passivating hydrogens and that, with respect to the edge-bbondings d_E , TV and BC states display respectively a bonding and an antibonding character.

B. ABNNRs

The gapwidth of ABNNRs fall in the same three families with the same hierarchy^{17,18,28}. This similarity with the graphene ribbons is actually quite general and can be understood from a simple tight-binding model (see section IV B). The evolution of the ABN-

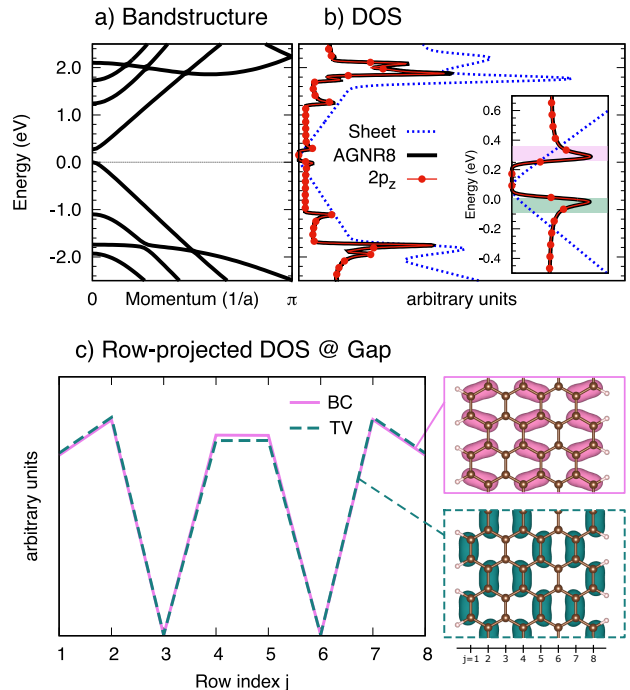


Figure 3. Electronic structure of the relaxed AGNR8. a) Band structure. b) and Inset: Total density of states (thick black) and projected on p_z orbital character (red bullets) compared with the DOS of the graphene sheet (dashed blue). c) Row-projected DOS from the integration of the total DOS around the band-edge states (shaded areas of panel b) and charge density associated with the TV and BC states at Γ .

NRs gapwidth for sizes going from $N_a=5$ to 19 in the relaxed and non-relaxed configurations is presented in Figure 4 by the solid blue and the red dashed lines. The non-relaxed structures present a gap that monotonically tends to the limit $N_a \rightarrow \infty$ in a way that is similar to non-passivated calculations¹⁷. We estimate $N_a \rightarrow \infty = 3.885$ eV from the weighted average of the curves extrapolated at $1/N_a = 0$ (cfr. inset of the Figure). This value is about 0.8 eV lower than the gapwidth of the isolated BN sheet (4.69 eV in PBE). All these aspects are consistent because, as it will become clearer later, in non-relaxed calculation, H atoms are too far to saturate efficiently the dangling bonds located at the edges of the ribbon. As a consequence, these form edge states inside the gap that lower the gapwidth similarly to what happens in non-passivated (bare) ribbons.

As a result of the structural optimisation, the gapwidth of all families opens and tends to an asymptotic limit that is still about 0.1 eV lower than in the isolated monolayer, in agreement with similar calculations^{14,17}. This discrepancy is ascribed to a non-negligible edge contribution to the BC state, obviously absent in the isolated monolayer (cfr. the row-projected DOS analysis here below, and¹⁴). Finally, we note that the first empty σ state, i.e. the near free-electron state, is only 0.5 eV above the BC.

Similarly to what done before, in Figure 5 we report the band structure, the projected DOS and the row-resolved DOS of the TV and BC states of the

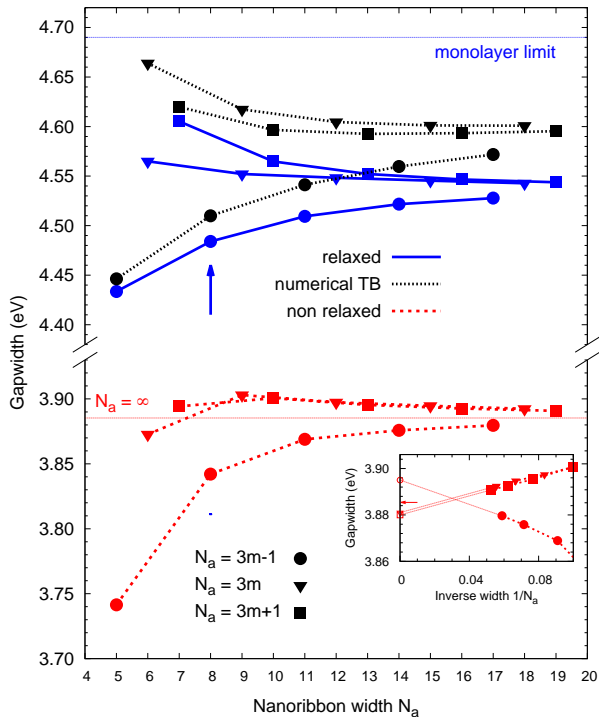


Figure 4. Energy gap of BN nanoribbons as a function of the size N_a . Relaxed DFT (blue solid line), unrelaxed (red dashed line) and the numerical tight-binding solution (Table I). The three families are reported with different symbols. Horizontal dashed lines indicate the gapwidth of the DFT hBN sheet (4.69 eV) and the asymptotic $N_a = \infty$ limit (~ 3.885 eV). The blue arrow pointing at the ABNNR8 indicates the system analysed in Figure 4. Inset: extrapolation of non-relaxed calculations at $1/N_a = 0$. The red arrow in the inset indicates the $N_a = \infty$ limit as the weighted average of the extrapolation of the three families.

representative ABNNR8 system. We verify that the TV and the BC states are formed essentially of N-centered and B-centered p_z orbitals respectively. The row-projected DOS of both TV and BC, reported in panel c), shows again a very nice static-wave-like modulation with nodes in rows 3 and 6, but at variance with the AGNR8 case, here the TV and BC states localize differently: while the TV states are delocalised on the entire nanoribbon as in the previous case, the BC states are clearly peaked at the edges. The visualization of the associated charge density confirms that the TV state is characterised by a wavefunction equally delocalised on all the N atoms except those on rows 3 and 6. Instead, the BC state presents a wavefunction more concentrated on the edge B atoms with non negligible tails touching passivating H and edge nitrogens, in contrast to the isolated monolayer.

The compared study of the TV and BC states of AGNRs and ABNNRs suggests that the gap of the two materials responds differently to modifications of the morphology and the passivation of the edges. To test this intuition, we have performed a detailed analysis by separating the two effects.

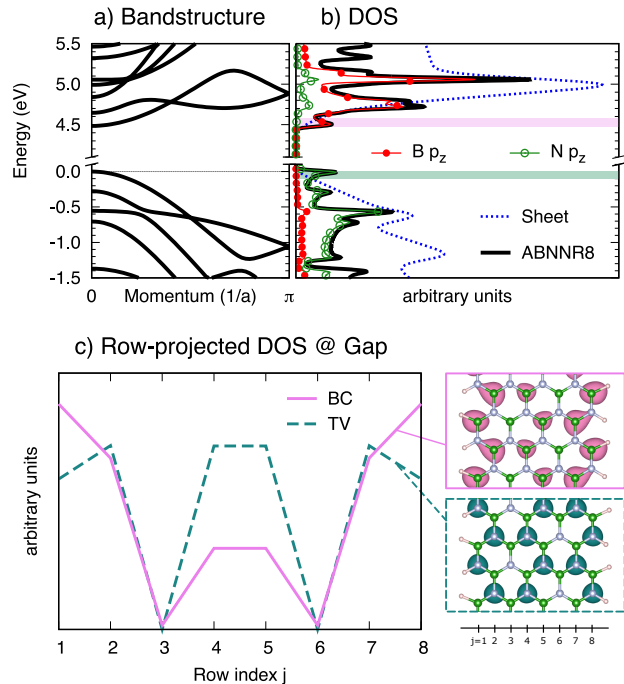


Figure 5. Electronic structure of the relaxed ABNNR8. a) band structure; b) total density of states (thick black) and projected on p_z orbital character (red and green dotted for B and N states) compared to the hBN sheet DOS (dashed blue). c) Row-projected DOS integrated around the band-edge states (shaded areas of panel b). Insets: charge density of the TV and BC states at Γ .

IV. MORPHOLOGY VS CHEMISTRY OF THE EDGES

A. Distinguishing the effects through selective relaxation in DFT

Several investigations can be found in literature on the effects of edge reconstruction on the gapwidth of AGNR and ABNNR^{6,12,17,19,21–26}. However, a study that systematically compares the effects of passivation and edge morphology is absent. Here we monitor the gapwidth in the family $N_a = 3m - 1$ by relaxing separately the H-X distances d_{HX} ($X = C, B$ or N) and the C-C or B-N distance on the edges d_E . We did calculate data from the other two families but we do not report them because they have qualitatively the same behaviour.

In Figure 6, a variation of d_{HX} is represented by a change in the line's type (color and dash), while a variation of d_E is represented by a change in the symbols (colour filled or empty). Let us examine first the case of AGNRs in panel a). We can start from a non-relaxed configuration where all atoms are equidistant $d_{HC}=d_E=1.42$ Å (empty bullets, red dashed line), then we reduce d_{HC} to its relaxed value 1.08 Å (empty bullets, blue solid line). We observe that there is basically no variation on the AGNRs' gapwidth. Instead, contracting the edge bonds from $d_E=1.42$ Å to $d_E=1.36$ Å opens the gap by around 0.15 eV irrespective of the value of d_{HC} . Consequently, we conclude

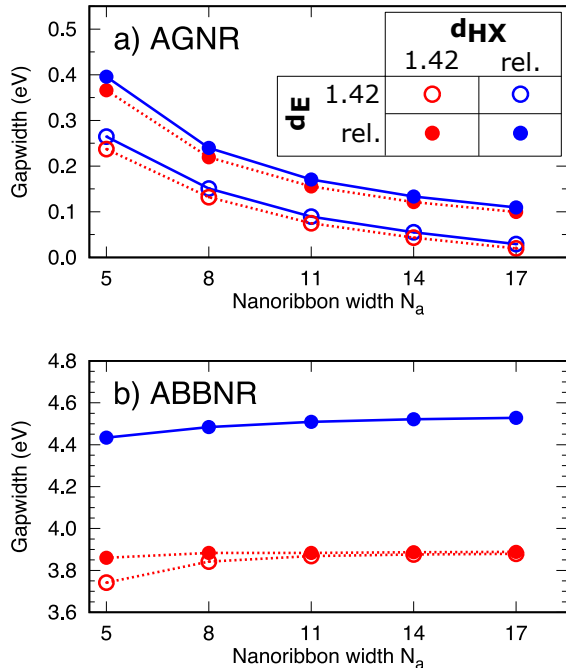


Figure 6. Gapwidth of the $N_a = 3m - 1$ family of a) AGNRs and b) ABNNRs. Full (empty) symbols stand for relaxed (non-relaxed) edge-atom bondings. Blue solid (red dashed) lines for relaxed (non-relaxed) passivating-to-edge-atoms bondings.

that in AGNRs, the variations of the gapwidth induced by the relaxation and reported in Figure 2 are essentially due to changes of bond length d_E between C atoms at the edge. Interestingly, this gap opening is approximately independent on the width of the ribbon.

Passing now to the study of ABNNRs (bottom panel), we observe an opposite behaviour. The gapwidth undergoes very small changes upon relaxation of d_E , whereas the passage from the unrelaxed H-B and H-N distance (1.42 Å) to the relaxed values clearly opens the gap by about 0.8 eV. To be more precise, by changing separately the two distances d_{HB} and d_{HN} (not shown), we found that it is the bonding between H and B that plays a major role in the opening of the gapwidth, indicating a dominant contribution from conduction states consistently with the observations we drew from Figure 5. According to this analysis, the gapwidth of ABNNRs is more sensitive to the passivation than to the very morphology of the edge. Once again we notice that the gap opening is basically independent on N_a . This clarifies why our non-relaxed DFT gapwidth look very similar to the non-passivated results of Topsakal and coworkers¹⁷.

B. Unperturbed tight-binding model

To investigate further the reasons of this different behaviour, we generalise a ladder tight-binding model introduced initially for AGNRs to the heteroatomic case. Changes in the edge passivation and morphology will be successively introduced through variations of

the on-site and hopping parameters of the model, as suggested in^{6,12}, and the modified Hamiltonian solved both numerically and perturbatively¹².

Following references^{6-8,10,12,16,20}, the gap of an armchair nanoribbon whose TV and BC states are formed of p_z orbitals can be described with a ladder tight-binding model as the one reported in Figure 7. The Hamiltonian of the model reads:

$$H^0 = \sum_{j,\mu} \left(\epsilon_{\mu j} |\Phi_{\mu j}\rangle + \sum_{j',\mu'} t_{\mu\mu'jj'} |\Phi_{\mu'j'}\rangle \right) \langle \Phi_{\mu j} |. \quad (1)$$

The index $j \in [1, N_a]$ labels the position of a dimer in the x coordinate (row coordinate), while $\mu = 1, 2$ indicates the atomic site within the dimer (C_1 or C_2 in AGNRs and B or N in ABNNRs). The basis function $\langle r | \Phi_{\mu j} \rangle = \Phi_{\mu}(\mathbf{r} - \mathbf{r}_j)$ is the p_z orbital of the atom μ of the dimer placed at $\mathbf{r}_j = \hat{x}(j-1)a$. For $\mu = 1$, $\Phi_{\mu}(\mathbf{r} - \mathbf{r}_j)$ is centered on the bottom rung if j is odd and in the upper rung if j is even, and the opposite for $\mu = 2$.

At the unperturbed level, $\epsilon_{\mu j}$ does not depend on the row-index j and is equal to ϵ for $\mu = 1$ and $-\epsilon$ for $\mu = 2$, with $\epsilon \geq 0$. In the first-neighbour approximation, the hopping term $t_{\mu\mu'jj'} = t \in \mathbb{R}$ if $\mu \neq \mu'$ and $j-1 \leq j' \leq j+1$ and vanishes otherwise. The unperturbed solutions of this model are:

$$E_{n\pm}^0 = \pm \sqrt{\epsilon^2 + \tau_n^2} = \pm \mathcal{E}_n, \quad (2)$$

where $\tau_n = t[1 + 2 \cos(\theta_n)]$, the discrete index n comes from the confinement in the x direction and $\theta_n = n\pi/(N_a + 1)$. The eigenfunction associated to these states read

$$\Psi_{n\pm} = \sum_{j=1}^{N_a} \sum_{\mu=1,2} \sin(j\theta_n) D_{\mu}^{n\pm} \Phi_{\mu}(\mathbf{r} - \mathbf{r}_j) \quad (3)$$

with

$$D_1^{n\pm} = \sqrt{\frac{\mathcal{E}_n \pm \epsilon}{(N_a + 1)\mathcal{E}_n}} \quad (4)$$

$$D_2^{n\pm} = \pm \text{sgn}(\tau_n) \sqrt{\frac{\mathcal{E}_n \mp \epsilon}{(N_a + 1)\mathcal{E}_n}}$$

where the function $\text{sgn}(x) = 1$ if $x \geq 0$ and -1 if $x < 0$. At this point, it is worth stressing two aspects. First, if one poses $\tau_n = 0$, then the Hamiltonian becomes diagonal and equivalent to that of a

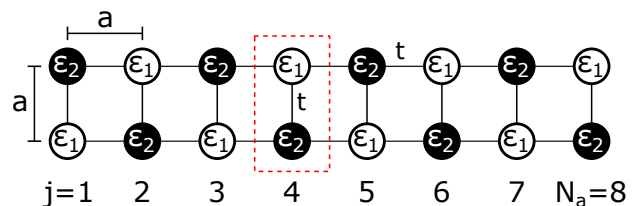


Figure 7. Scheme of the ladder model of width $N_a = 8$. The first neighbours distance is a , the index j defines the position of a dimer. Atoms $\mu = 1$ are placed above $\mu = 2$ if j is even, below if j is odd.

non-interacting system. Consistently, the coefficients $D_\mu^{n\pm}$ become those of a pure system: $D_1^{n+} = -D_2^{n-} = \sqrt{2/(N_a + 1)}$ and $D_1^{n-} = D_2^{n+} = 0$. If instead one takes the homoatomic limit, i.e. $\epsilon \rightarrow 0$, then the coefficients become a bonding and antibonding pair, with $D_1^{n\pm} = 1/\sqrt{N_a + 1}$ and $D_2^{n\pm} = \pm \text{sgn}(\tau_n)/\sqrt{N_a + 1}$.

The last occupied state (TV) $|\tilde{n}, -\rangle$ and the first empty state (BC) $|\tilde{n}, +\rangle$ are found at the integer quantum number \tilde{n} that minimizes the quantity \mathcal{E}_n , i.e. that minimize $|\tau_n|$. If $N_a = 3m$ or $3m+1$ with $m \in \mathbb{N}^*$, then $\tilde{n} = 2m+1$. Note that the interacting term τ_{2m+1} changes sign in passing from one family to the other. Instead if $N_a = 3m - 1$, then the integer $\tilde{n} = 2m$ and $\tau_n = 0$. These considerations leads to the unperturbed gap of a heteroatomic system ($\epsilon > 0$):

$$\Delta_{N_a}^0 = \begin{cases} 2\epsilon & \text{for } N_a = 3m - 1 \\ 2\mathcal{E}_{2m+1} & \text{for the other values of } N_a \end{cases} \quad (5)$$

and the eigenstates of the TV and BC of the $N_a = 3m - 1$ family are pure states. The gap of a homoatomic system ($\epsilon = 0$) reads:

$$\Delta_{N_a}^0 = \begin{cases} 0 & \text{for } N_a = 3m - 1 \\ 2|\tau_{2m+1}| & \text{for the other values of } N_a \end{cases} \quad (6)$$

and the eigenstates of the TV and BC of the $N_a = 3m - 1$ family are the bonding and antibonding combinations of C_1 and C_2 .

C. Distinguishing the effects through perturbation theory

As in^{6,12}, we now add to H^0 a perturbation Hamiltonian δH which consists in adding δt to the hopping term connecting the atoms of the edge rows ($j = 1, N_a$) and in changing their on-side energy by $\delta\epsilon_\mu$. The hopping perturbation δt accounts for changes in d_E , so it is more strongly related to the edge morphology, while the on-site one $\delta\epsilon$ takes into account variations of d_{HX} and of the passivating species. The perturbative correction to the energy of the generic state $|n\pm\rangle$ reads

$$\langle n, \pm | \delta H | n, \pm \rangle = 2 \sin^2(\theta_n) \times \left[(D_1^{n\pm})^2 \delta\epsilon_1 + (D_2^{n\pm})^2 \delta\epsilon_2 + 2D_1^{n\pm} D_2^{n\pm} \delta t \right] \quad (7)$$

In the heteroatomic case $\epsilon > 0$, the perturbative correction to the gap is always $\delta\Delta = \langle \tilde{n}, + | \delta H | \tilde{n}, + \rangle - \langle \tilde{n}, - | \delta H | \tilde{n}, - \rangle$. Using (7), the coefficients (4) or their appropriate limit, and remembering that $\Delta_{N_a}^0 = 2\mathcal{E}_{\tilde{n}}$, then the gap correction for the case $\epsilon > 0$ reads,

$$\delta\Delta = (\delta\epsilon_1 - \delta\epsilon_2) / m \quad (8)$$

for $N_a = 3m - 1$; and

$$\delta\Delta = \frac{8 \sin^2(\theta_{2m+1})}{(N_a + 1) \Delta^0} \times \left[\epsilon (\delta\epsilon_1 - \delta\epsilon_2) + 2\tau_{2m+1} \delta t \right] \quad (9)$$

for $N_a = 3m$ and $N_a = 3m + 1$. Notice that, by construction, τ_{2m+1} is the closest to zero among the accessible values, so the term $2\tau_{2m+1} \delta t$ is always negligible. The result shows that in ABNNRs the variations of the gap are mostly due to the chemical environment of the edge atoms. This dependence comes ultimately from an interference between the TV and the BC wavefunctions. These two states are very close to pure states, so the mixed products $D_1^+ D_2^+$ and $D_1^- D_2^-$ of equation (7) are systematically negligible, and they do actually vanish in the family $N_a = 3m - 1$ where the two states are perfectly pure.

In the homoatomic case ($\epsilon = 0$) the corrected gap can be obtained following the same approach as before, and taking the appropriate limits of the coefficients (4). However, more attention must be paid in studying the family $N_a = 3m - 1$. In fact this case corresponds to the double limit $\epsilon \rightarrow 0$ and $\tau_n \rightarrow 0$. Even though the final eigenvalues do not depend on the order with which the two limits are taken, the eigenstates do, therefore also the perturbative corrections depend on this choice. In DFT calculation and experiments, the system itself is well defined at the very first place, because one works either with ABNNRs or with AGNRs. So, for comparisons with DFT to make sense, the right order with which the limits must be taken is: first $\epsilon \rightarrow 0$, followed by $\tau_n \rightarrow 0$. Finally, one has to pay attention to another point: in the $N_a = 3m - 1$ family, the TV and the BC states are degenerate and the unperturbed gap is 0. So there is no reason to define $\delta\Delta = \langle \tilde{n}, + | \delta H | \tilde{n}, + \rangle - \langle \tilde{n}, - | \delta H | \tilde{n}, - \rangle$ rather than its opposite. However, the correction must be positive, so the correction must be defined as the modulus of the difference above. Putting all these things together, one gets for the homoatomic ($\epsilon = 0$) case

$$\delta\Delta = \begin{cases} \frac{2}{m} |\delta t| & \text{for } N_a = 3m - 1 \\ \text{sgn}(\tau_{2m+1}) \frac{8 \sin^2(\theta_{2m+1})}{(N_a + 1)} \delta t & \text{otherwise} \end{cases} \quad (10)$$

This result shows that in AGNRs most of the variations of the gap is accounted by δt , so by morphological changes of the bonding between edge atoms, and not by changes of their chemical environment. Once again this result can be understood from the symmetries of the TV and BC wavefunctions. In fact, when $\epsilon = 0$, the TV and BC states are perfect bonding and antibonding combinations at any N_a , so their difference causes the terms in $(D_\mu^{n\pm})^2$ of equation (7) to always cancel out. This result, although in perfect agreement with¹², seems to be in blatant contradiction with results from 2H-passivated AGNRs²⁶, where the gap is found independent on the C-C edge distance. Actually, these systems present a hybridisation of the sp^3 type and their gapwidth can not be described by this model.

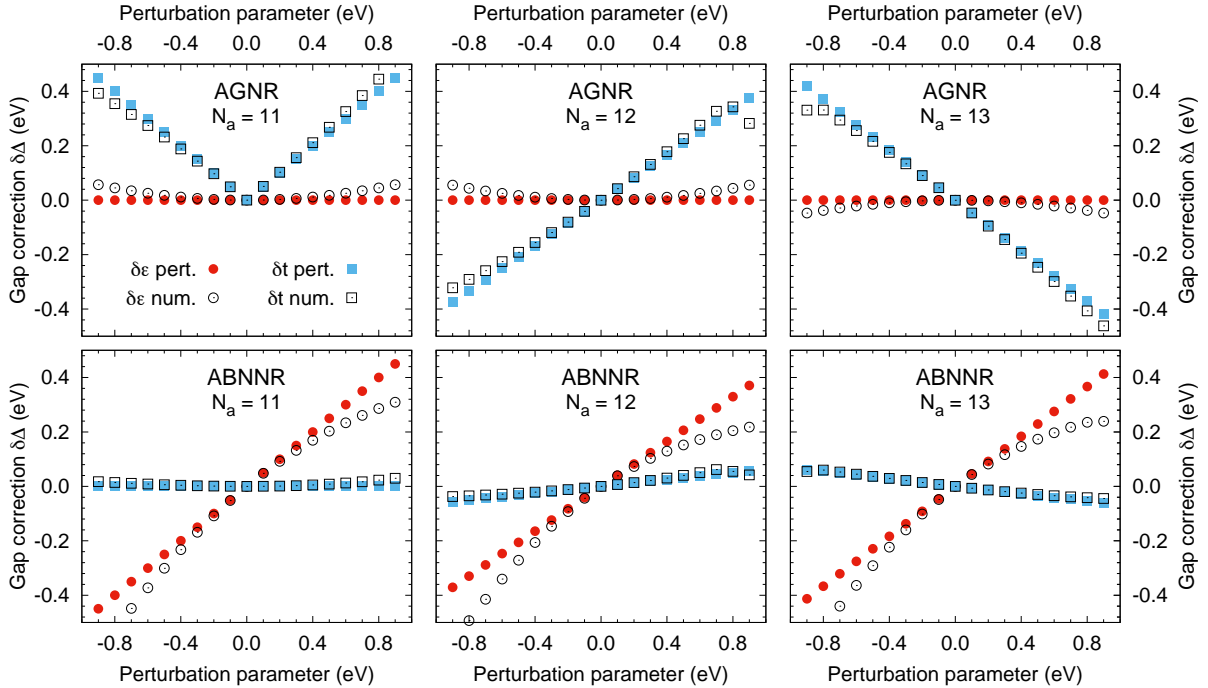


Figure 8. Deviation from $\Delta_{N_a}^0$ as a function of δt (squares) or $\delta\epsilon$ (circles) in AGNRs (top panels) and ABNNRs (bottom panels). From left to right: $N_a = 11, 12, 13$. Colored symbols result from equations (8 - 10); empty symbols from the numerical solution.

D. Validation of the perturbative approach

Besides the perturbative approach, we also solved the perturbed Hamiltonian $H = H^0 + \delta H$ numerically. For the unperturbed problem, we parametrized the model with values that fit the band structure of the isolated graphene and hBN monolayers. Instead, the perturbation parameters $\delta\epsilon$ and δt have been adjusted to recover as best as possible the DFT curves reported in Figures 2 and 4. The best parameters are reported in Table I. Successively we explored how the gap changes upon variations of the perturbative parameters δt and $\delta\epsilon_\mu$ in the range -1 eV, +1 eV in the nanoribbons of width $N_a=11, 12$ and 13, i.e. one representative nanoribbon per family. Guided by physical intuitions we took $\delta\epsilon_1 = \delta\epsilon_2 = \delta\epsilon$ in the case of AGNRs, and $\delta\epsilon_1 = -\delta\epsilon_2 = \delta\epsilon$ in the case of ABNNRs.

Globally, the numerical and the perturbative gapwidth are in very good agreement for both ABNNRs and AGNRs in the range explored, confirming our conclusions. In all cases, the numerical solution displays a quadratic trend with respect to $\delta\epsilon$ which adds on top of the invariance (AGNR) or the linear (ABNNR) dependence predicted by the perturbative approach. The deviations between the two approaches are larger

AGNR			ABNNR			
ϵ_C	t_{CC}	δt	ϵ_B	ϵ_N	t_{BN}	$\delta\epsilon$
0.0	-2.6	-0.4	2.32	-2.32	-2.46	-0.3

Table I. Parameters of $H = H^0 + \delta H$ in eV used to plot curves in Figures 2 and 4.

for this parameter than for δt , with the larger deviations of the order of 0.2 eV in the $N_a = 3m$ and $N_a = 3m + 1$ families of ABNNRs. Instead, the deviations for the parameter δt are in general very small and never larger than 0.1 eV. Note however that for extreme values of δt , the numerical solution may undergo a band crossing in the top valence and the bottom conduction which would lead to a sudden closing of the gap, as it is the case at $\delta t = -0.9$ in AGNR13 and $\delta t = 0.9$ in AGNR12. This physics is not accessible in our first order expansion and clearly sets the limit of applicability of the perturbative approach.

V. CONCLUSION

We have calculated with DFT the gapwidth of graphene and boron nitride armchair nanoribbons (AGNRs and ABNNRs) for ribbon sizes going from $N_a = 5$ rows to $N_a = 19$ rows both for relaxed and unrelaxed structures. We have relaxed selectively specific interatomic distances and reported how the gapwidth changes upon variations of the bondlength with passivating atoms (chemistry-driven changes) and between edge atoms (morphology-driven changes). Thanks to this selective relaxation, we showed that the variations of the gapwidth in AGNRs are morphology-driven, while in ABNNRs are chemistry-driven. To understand why, we adopted and extended the tight-binding approach introduced by Son and coworkers¹² and we demonstrated that the interference between the wavefunctions of the top valence and the bottom conduction are at the origin of these two distinct responses.

In the AGNR case, these states are basically a bonding and antibonding pair. As the two states are equally distributed on the atoms, the difference between BC and TV leads to a mutual cancellation of on-site changes, and only hopping terms survive. This explains the stronger dependence of the gapwidth on interatomic distances and hence on the morphology of the edges rather than the chemical environment. At variance, in ABNNR case, the TV and the BC states

are basically pure states and the effective Hamiltonian is quasi-non-interacting. As a result, the two states are mostly insensitive to variations in the hopping term and are instead strongly affected by on-site variations (chemical environment).

Our results can help pushing further the research on nanoribbon-based devices, as they clarify the role played by edge-engineering, and selective passivation and provide the tools to investigate more complex scenarios.

-
- ¹ A. K. Geim and K. S. Novoselov, *Nature Materials* **6**, 183 (2007).
- ² K. Watanabe, T. Taniguchi, T. Niiyama, K. Miya, and M. Taniguchi, *Nature Photonics* **3**, 591 (2009).
- ³ A. H. Castro Neto, F. Guinea, N. M. R. Peres, K. S. Novoselov, and A. K. Geim, *Reviews of Modern Physics* **81**, 109 (2009), arXiv:0709.1163.
- ⁴ Q. Weng, X. Wang, X. Wang, Y. Bando, and D. Golberg, *Chemical Society Reviews* **45**, 3989 (2016).
- ⁵ K. Zhang, Y. Feng, F. Wang, Z. Yang, and J. Wang, *Journal of Materials Chemistry C* **5**, 11992 (2017).
- ⁶ M. Ezawa, *Phys. Rev. B* **73**, 045432 (2006).
- ⁷ M. Fujita, K. Wakabayashi, K. Nakada, and K. Kusakabe, *Journal of the Physical Society of Japan* **65**, 1920 (1996).
- ⁸ K. Nakada, M. Fujita, G. Dresselhaus, and M. S. Dresselhaus, *Phys. Rev. B* **54**, 17954 (1996).
- ⁹ S. Behzad and R. Chegel, *Diamond and Related Materials* **88**, 101 (2018).
- ¹⁰ K. Wakabayashi, M. Fujita, H. Ajiki, and M. Sigrist, *Physical Review B* **59**, 8271–8282 (1999).
- ¹¹ L. Yang, C.-H. Park, Y.-W. Son, M. L. Cohen, and S. G. Louie, *Physical Review Letters* **99**, 186801 (2007), arXiv:0706.1589.
- ¹² Y.-W. Son, M. L. Cohen, and S. G. Louie, *Physical Review Letters* **97**, 216803 (2006).
- ¹³ J. Nakamura, T. Nitta, and A. Natori, *Phys. Rev. B* **72**, 205429 (2005).
- ¹⁴ C.-H. Park and S. G. Louie, *Nano Letters* **8**, 2200 (2008), pMID: 18593205, <https://doi.org/10.1021/nl080695i>.
- ¹⁵ S. Wang, Q. Chen, and J. Wang, *Applied Physics Letters* **99**, 063114 (2011).
- ¹⁶ F.-L. Shyu, *Physica B: Condensed Matter* **452**, 7 (2014).
- ¹⁷ M. Topsakal, E. Aktürk, and S. Ciraci, *Physical Review B* **79**, 115442 (2009).
- ¹⁸ Z. Zhang and W. Guo, *Physical Review B* **77**, 075403 (2008).
- ¹⁹ Y. Ding, Y. Wang, and J. Ni, *Applied Physics Letters* **94**, 233107 (2009).
- ²⁰ H. Nematian, M. Moradinasab, M. Pourfath, M. Fathipour, and H. Kosina, *Journal of Applied Physics* **111**, 093512 (2012).
- ²¹ V. Barone, O. Hod, and G. E. Scuseria, *Nano Letters* **6**, 2748 (2006).
- ²² K. K. Jha, N. Tyagi, N. K. Jaiswal, and P. Srivastava, *Physics Letters A* **383**, 125949 (2019).
- ²³ V. K. Nishad, A. K. Nishad, S. Roy, B. K. Kaushik, and R. Sharma, *Proceedings of the IEEE Conference on Nanotechnology 2020-July*, 155 (2020).
- ²⁴ S. Prabhakar and R. Melnik, *Physica E: Low-dimensional Systems and Nanostructures* **114**, 113648 (2019).
- ²⁵ H. Ren, Q. Li, H. Su, Q. W. Shi, J. Chen, and J. Yang, arXiv, 0711.1700 (2007), arXiv:0711.1700.
- ²⁶ Y. Lu, R. Wu, L. Shen, M. Yang, Z. Sha, Y. Cai, and Y. Feng, *Applied Physics Letters* **94**, 122111 (2009).
- ²⁷ H. Raza and E. C. Kan, *Phys. Rev. B* **77**, 245434 (2008).
- ²⁸ J. Li, L. Z. Sun, and J. X. Zhong, *Chinese Physics Letters* **27**, 077101 (2010).
- ²⁹ P. Zheng, S. E. Bryan, Y. Yang, R. Murali, A. Naeemi, and J. D. Meindl, *IEEE Electron Device Letters* **34**, 707 (2013).
- ³⁰ R. Murali, Y. Yang, K. Brenner, T. Beck, and J. D. Meindl, *Applied Physics Letters* **94**, 243114 (2009).
- ³¹ S. Das, S. Bhattacharya, D. Das, and H. Rahaman, *AIMS Materials Science* **8**, 247 (2021).
- ³² J. M. Marmolejo-Tejada and J. Velasco-Medina, *Microelectronics Journal* **48**, 18 (2016).
- ³³ V. Saraswat, R. M. Jacobberger, and M. S. Arnold, *ACS Nano* **15**, 3674 (2021).
- ³⁴ S. Osella, A. Narita, M. G. Schwab, Y. Hernandez, X. Feng, K. Mullen, and D. Beljonne, *ACS nano* **6**, 5539 (2012).
- ³⁵ M. Mehdi Pour, A. Lashkov, A. Radocea, X. Liu, T. Sun, A. Lipatov, R. A. Korlacki, M. Shekhirev, N. R. Aluru, J. W. Lyding, V. Sysoev, and A. Sinitskii, *Nature Communications* **8**, 820 (2017).
- ³⁶ M. G. Schwab, A. Narita, S. Osella, Y. Hu, A. Maghsoumi, A. Mavrinsky, W. Pisula, C. Castiglioni, M. Tommasini, D. Beljonne, X. Feng, and K. Müllen, *Chemistry – An Asian Journal* **10**, 2134 (2015), <https://onlinelibrary.wiley.com/doi/pdf/10.1002/asia.201500450>.
- ³⁷ G. Wang, S. Wu, T. Zhang, P. Chen, X. Lu, S. Wang, D. Wang, K. Watanabe, T. Taniguchi, D. Shi, R. Yang, and G. Zhang, *Applied Physics Letters* **109**, 053101 (2016), <https://doi.org/10.1063/1.4959963>.
- ³⁸ J. Dauber, B. Terrés, C. Volk, S. Trellenkamp, and C. Stampfer, *Applied Physics Letters* **104**, 083105 (2014), <https://doi.org/10.1063/1.4866289>.
- ³⁹ B. Huang, M. Liu, N. Su, J. Wu, W. Duan, B.-I. Gu, and F. Liu, *Phys. Rev. Lett.* **102**, 166404 (2009).
- ⁴⁰ B. Huang, H. Lee, B. L. Gu, F. Liu, and W. Duan, *Nano Research* **5**, 62 (2012).
- ⁴¹ J. P. Perdew, K. Burke, and M. Ernzerhof, *Physical Review Letters* **77**, 3865 (1996).
- ⁴² P. Giannozzi, S. Baroni, N. Bonini, M. Calandra, R. Car, C. Cavazzoni, D. Ceresoli, G. L. Chiarotti, M. Cococcioni, I. Dabo, *et al.*, *Journal of physics: Condensed matter* **21**, 395502 (2009).
- ⁴³ S. Grimme, *Journal of Computational Chemistry* **27**, 1787 (2006), <https://onlinelibrary.wiley.com/doi/pdf/10.1002/jcc.20495>.
- ⁴⁴ D. R. Hamann, *Phys. Rev. B* **88**, 085117 (2013).

- ⁴⁵ M. Posternak, A. Baldereschi, A. J. Freeman, E. Wimmer, and M. Weinert, Phys. Rev. Lett. **50**, 761 (1983).
- ⁴⁶ M. Posternak, A. Baldereschi, A. J. Freeman, and E. Wimmer, Phys. Rev. Lett. **52**, 863 (1984).
- ⁴⁷ X. Blase, A. Rubio, S. G. Louie, and M. L. Cohen, Physical Review B **51**, 6868 (1995).
- ⁴⁸ F. Paleari, *First-principles approaches to the description of indirect absorption and luminescence spectroscopy: exciton-phonon coupling in hexagonal boron nitride*, Ph.D. thesis, University of Luxembourg (2019).
- ⁴⁹ S. Latil, H. Amara, and L. Sponza, “Structural classification of boron nitride twisted bilayers and ab initio investigation of their stacking-dependent electronic structure,” (2022), accepted in SciPost Physics.
- ⁵⁰ X. Blase, L. X. Benedict, E. L. Shirley, and S. G. Louie, Phys. Rev. Lett. **72**, 1878 (1994).
- ⁵¹ X. Blase, A. Rubio, S. G. Louie, and M. L. Cohen, Europhysics Letters (EPL) **28**, 335 (1994).
- ⁵² S. Hu, J. Zhao, Y. Jin, J. Yang, H. Petek, and J. G. Hou, Nano Letters **10**, 4830 (2010), pMID: 21049977, <https://doi.org/10.1021/nl1023854>.